

An open circuit voltage decay system for performing injection dependent lifetime spectroscopy

Shelby Lacouture,¹ James Schrock,¹ Emily Hirsch,¹ Stephen Bayne,¹ Heather O'Brien,² and Aderinto A. Ogunniyi²

¹Department of Electrical Engineering, Texas Tech University, 1012 Boston Ave., Lubbock, Texas 79409, USA

²U.S. Army Research Laboratory, Adelphi, Maryland 20783, USA

(Received 18 April 2017; accepted 24 August 2017; published online 14 September 2017)

Of all of the material parameters associated with a semiconductor, the carrier lifetime is by far the most complex and dynamic, being a function of the dominant recombination mechanism, the equilibrium number of carriers, the perturbations in carriers (e.g., carrier injection), and the temperature, to name the most prominent variables. The carrier lifetime is one of the most important parameters in bipolar devices, greatly affecting conductivity modulation, on-state voltage, and reverse recovery. Carrier lifetime is also a useful metric for device fabrication process control and material quality. As it is such a dynamic quantity, carrier lifetime cannot be quoted in a general range such as mobility; it *must* be measured. The following describes a stand-alone, wide-injection range open circuit voltage decay system with unique lifetime extraction algorithms. The system is initially used along with various lifetime spectroscopy techniques to extract fundamental recombination parameters from a commercial high-voltage PIN diode. Published by AIP Publishing. [<http://dx.doi.org/10.1063/1.5001732>]

I. INTRODUCTION

The most widely ranging and dynamic material parameter of a semiconductor is by far the carrier lifetime; this material parameter cannot be given as even a rough figure like the carrier mobility: it is a complex quantity that depends on a multitude of factors and it changes with every single processing step a device undergoes. Carrier lifetime has a profound effect on the characteristics of many solid-state devices; prime examples for power semiconductors include the on-state voltage and reverse-recovery time of devices that rely on conductivity modulation.¹ These two characteristics alone make carrier lifetime of paramount importance in high-voltage PIN rectifiers, insulated-gate bipolar transistors (IGBTs), and thyristors. Being able to accurately measure the carrier lifetime and the recombination activity of various defects introduced into a semiconductor's lattice not only allows accurate device modeling² and gives insight into the effect of carrier lifetime on a device's external performance³ but this information can be used as a process control metric when combined with wafer-level lifetime measurement techniques. Although Deep Level Transient Spectroscopy (DLTS)⁴ is the most commonly accepted measurement technique for characterizing defects in pn junctions, the technique can miss defects that exist in concentrations below the detection limit of the method, even though such defects can still greatly affect carrier lifetime, e.g., monocrystalline Czochralski.⁵ DLTS also gives no information on the carrier lifetime itself. A relatively new set of techniques that use the Shockley-Read-Hall (SRH) theory⁶ are collectively known as Lifetime Spectroscopy (LS) and offer a very sensitive method of specifically characterizing defects that strongly affect carrier lifetime, and since the effective lifetime itself is the primary quantity measured, these methods can be utilized to fill in missing data about the recombination activity of particular defects in various semiconductors.

In order to accurately utilize these LS techniques, the effective lifetime, τ_{eff} , must be measured as exactly as possible. Toward this goal, a complete system was developed that precisely controls injected current into a junction over a wide range $\sim 1 \text{ mA} - 200 \text{ A}$ and uses built-in data acquisition to capture the decay waveforms produced. The Open Circuit Voltage Decay (OCVD) method was employed with a relatively unique data extraction algorithm that circumvents the inherent abstraction of data and added noise caused by conventional methodologies.

II. THEORETICAL BACKGROUND

The extraction of minority and majority carrier lifetimes and the energy depth of the dominant defect performed in this work relies on the LS methods mentioned in the Introduction. All LS methods are based upon applying the quantitative theories of carrier lifetime in a systematic way by varying the injection of carriers, the doping concentration, and/or the temperature while monitoring the effective lifetime. Sections II A and II B cover the very basics of LS techniques as well as the method used to measure the effective lifetime: the OCVD technique.

A. Lifetime spectroscopy techniques

Although there are several variations of LS, all the methods devised stem from the well-established SRH theory. The SRH lifetime expression for a p⁺n junction,⁶ provided in Eq. (1), is the starting point for developing the LS methods,

$$\tau_{\text{SRH}} = \tau_{n0} \left(\frac{p_0 + p_1 + \Delta n}{p_0 + n_0 + \Delta n} + k \frac{n_0 + n_1 + \Delta n}{p_0 + n_0 + \Delta n} \right), \quad (1)$$

where τ_{n0} is the minority carrier lifetime, p_0 and n_0 are the equilibrium carrier concentrations, p_1 and n_1 are the SRH densities,

Δn is the number of excess carriers, and k is a “symmetry” factor, defined by the following equation:

$$k = \frac{\tau_{p0}}{\tau_{n0}} = \frac{\sigma_n}{\sigma_p}. \quad (2)$$

Here, σ_n and σ_p are carrier capture cross sections. In the limit of low-level injection (LLI), defined as $\Delta n \ll n_0 + p_0$, the SRH equation simplifies to

$$\tau_{SRH}^{LLI} = \tau_{n0} \left(\frac{p_0 + p_1}{p_0 + n_0} + k \frac{n_0 + n_1}{p_0 + n_0} \right), \quad (3)$$

while in the limit of high-level injection (HLI) ($\Delta n \gg n_0 + p_0$), the SRH lifetime asymptotes to the ambipolar lifetime irrespective of the SRH densities (i.e., trap energy depth, E_t has no effect under HLI); mathematically this is given by

$$\tau_{SRH}^{HLI} = \tau_{n0} + \tau_{p0} = \tau_{n0} (1 + k). \quad (4)$$

Injection Dependent Lifetime Spectroscopy (IDLS) is based on the study of the shape and magnitude of the SRH lifetime over a wide injection of minority carriers. From such a curve, three quantitative parameters can be extracted with two of them being independent, specifically: τ_{LLI} , τ_{HLI} , and the difference $\Delta\tau_{SRH}$ can be measured. The shape of the IDLS curve is influenced by the defect energy level through the SRH densities. The general SRH expression, Eq. (1), models the entire IDLS curve and is a function of three variables: E_t (through n_1 and p_1), k , and τ_{n0} . The general SRH expression can be simplified, however, as shown in Eqs. (3) and (4). While these two relations originate from the general SRH equation, they are independent within their respective injection regimes. This then gives two independent equations in three unknowns. What can be expected from this is a solution surface rather than a set of discrete solutions; this continuum of solutions is termed the Defect Parameter Solution Surface (DPSS). The extractable parameters from a single (ideal) IDLS curve are $\tau_{SRH-LLI}$, $\tau_{SRH-HLI}$, and the difference of the two values $\Delta\tau_{SRH}$. An equation for this last quantity can be derived by subtracting Eq. (3) from Eq. (4), yielding

$$\Delta\tau_{SRH} = \tau_{n0} \left(\frac{n_0 - p_1}{p_0 + n_0} + k \frac{p_0 - n_1}{p_0 + n_0} \right). \quad (5)$$

Equation (5) is not independent of the two relations used to derive it, but can be combined with either of the other original equations to form an independent pair of equations.

To visualize the solution surface discussed above, Eqs. (3) and (5) are rewritten in terms of DPSS independent variables and then solved for two of these DPSS parameters, DPSS- k and DPSS- τ_{n0} ,

$$\tau_{n0}^{DPSS} = \frac{\Delta\tau_{SRH} (n_0 + n_1^{DPSS}) - \tau_{SRH}^{LLI} (p_0 - n_1^{DPSS})}{(n_0 + n_1^{DPSS}) - (p_0 + p_1^{DPSS})}, \quad (6)$$

and

$$k^{DPSS} = \frac{-(p_0 + n_0) + (p_0 + p_1^{DPSS}) \left(1 + \frac{\Delta\tau_{SRH}}{\tau_{SRH}^{LLI}} \right)}{(p_0 + n_0) - (n_0 + n_1^{DPSS}) \left(1 + \frac{\Delta\tau_{SRH}}{\tau_{SRH}^{LLI}} \right)}. \quad (7)$$

These two new equations then allow the DPSS curves, DPSS- k and DPSS- τ_{n0} , to be graphed as functions of the empirically extracted values, $\tau_{SRH-LLI}$ and $\Delta\tau_{SRH}$ (constants), and

the DPSS independent variables, n_1 -DPSS and p_1 -DPSS (and correspondingly the dependent variable, the DPSS energy level: E_t). These equations in effect give simultaneous solution curves for k and τ_{n0} over the range of defect energy levels that would directly result in the original IDLS curve from which $\tau_{SRH-LLI}$ and $\Delta\tau_{SRH}$ were obtained. Figure 1 shows these two solution surfaces for three levels of defect energy.

From Sec. II, it can be concluded that a single IDLS curve cannot produce unambiguous results. This does not mean IDLS is invalidated; it simply shows the need for more information to remove the inherent ambiguity arising from the lack of original defining equations. One way to remove the uncertainty of the DPSS IDLS analysis is to vary the LLI recombination of a center and thus vary the shape of an IDLS curve. This may be accomplished by varying the ratio n_1/p_0 or p_1/p_0 . These ratios can be altered either indirectly by varying the doping concentration, a method referred to as doping IDLS (N_{dop} -IDLS), or directly by varying the sample temperature, as the SRH densities n_1 and p_1 are relatively strong functions of temperature. This method is termed Temperature-Injection Dependent Lifetime Spectroscopy (T-IDLS). If the ratios can be varied enough, several k -DPSS curves, when plotted on the same graph, intersect at two points ($|E_t|$) on the energy axis that represent the true absolute energy depth of the center within a small degree of uncertainty.

In order to apply the T-IDLS method, the temperature dependence of the minority carrier lifetimes must also be taken into account. This dependence on temperature arises from two factors: the thermal velocity and the capture cross section. These factors lead to a general relationship for the minority carrier lifetime as a function of temperature,⁶

$$\tau_{n0}(T) = \tau_{n0}^{300K} \left(\frac{T}{300K} \right)^\alpha, \quad (8)$$

where alpha is the sum of the effects of the thermal velocity and the capture cross section.

The DPSS- τ_{n0} plots, unlike the DPSS- k graphs, do not intersect at discrete E_t solutions due to the variation of τ_{n0} with temperature: at the true energy depth, each curves' τ_{n0} is a different value. It is a simple matter however to model these variations in the DPSS- τ_{n0} plots with the use of Eq. (8), which then yields the minority lifetime as a function of temperature.

B. Open circuit voltage decay method

In order to apply the LS methods described above, the effective lifetime must be accurately measured over several orders of magnitude of carrier injection. The system described herein utilizes the OCVD technique to extract this effective lifetime from a pn junction. The method is completely electrical, is non-destructive, and requires only two connections via wires to the device, allowing ease of access to temperature chambers, etc. The OCVD method has grown in prominence over the last several years as a viable technique for extracting the effective lifetime from packaged pn junction devices. In many ways, it has been shown to be much more accurate than the various optical methods used for the same purpose,⁷

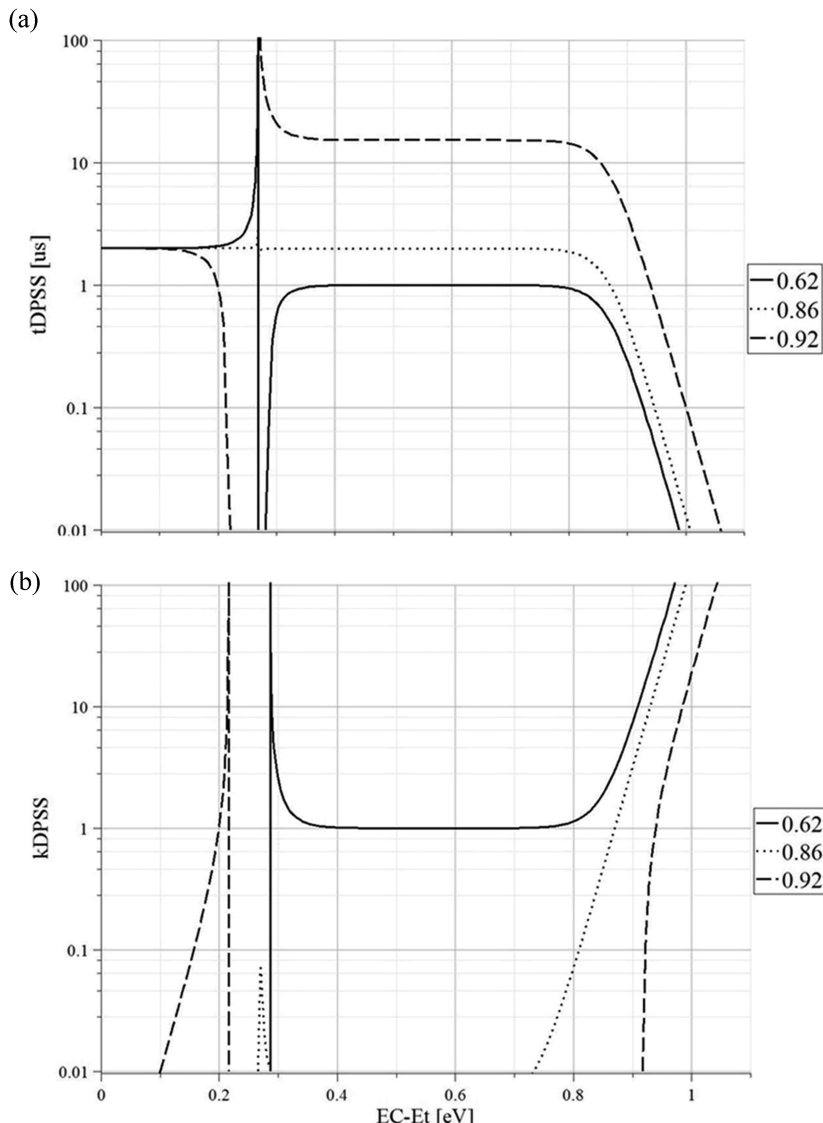


FIG. 1. DPSS t_{n0} (a) and k (b) for three true defect energy levels.

mostly due to the fact that the lifetime itself is the fundamental quantity measured with the OCVD technique, as opposed to extrapolating the lifetime from a sample's conductance, a quantity that can be greatly affected by carrier trapping. The OCVD technique is also generally accepted as being more accurate than other electrical methods such as Current Recovery Time (CRT).⁸ Several studies using mathematical simulations of pn junctions have shown very good correlation of the output OCVD signals with the recombination constants used in the simulations.⁹ The seemingly conflicting reports encountered in some of the studies are likely due to a lack of standardization and transparency in the methodology used in the actual physical experiments;¹⁰ even the method used to rapidly disconnect a pn junction can greatly affect the voltage decay and hence the extracted lifetime value.¹¹ The orthodox method of differentiating and filtering the OCVD waveforms to extract the lifetime is also somewhat problematic.

The OCVD method was first described by Lederhandler and Giacoletto.¹² In its simplest, most ideal form, a forward bias is applied for a finite time and then the junction is

disconnected (ideally, in as galvanic a manner as possible) from the source. Once the source is removed from the junction, the voltage across the diode immediately drops by an initial amount, ΔV , due to the junction's internal series resistance, and then the voltage decays (ideally, assuming no excessive parallel resistance or capacitance) due to recombination of the injected carriers. Equation (9) is derived by differentiating the voltage expression for a pn junction assuming asymmetrical doping. It can be shown that during periods where this function is a constant value (decay voltage is linear with respect to time), the slope of the voltage is inversely proportional to the effective lifetime,⁷

$$F(t) = -\eta \frac{kT}{q} \left(\frac{dv(t)}{dt} \right)^{-1}, \quad (9)$$

where k is Boltzmann's constant, T is the temperature in Kelvin, and η is the injection-dependent ideality factor calculated for a p^+n junction by the following equation:¹¹

$$\eta = 1 + \frac{\Delta p}{(p+n)}. \quad (10)$$

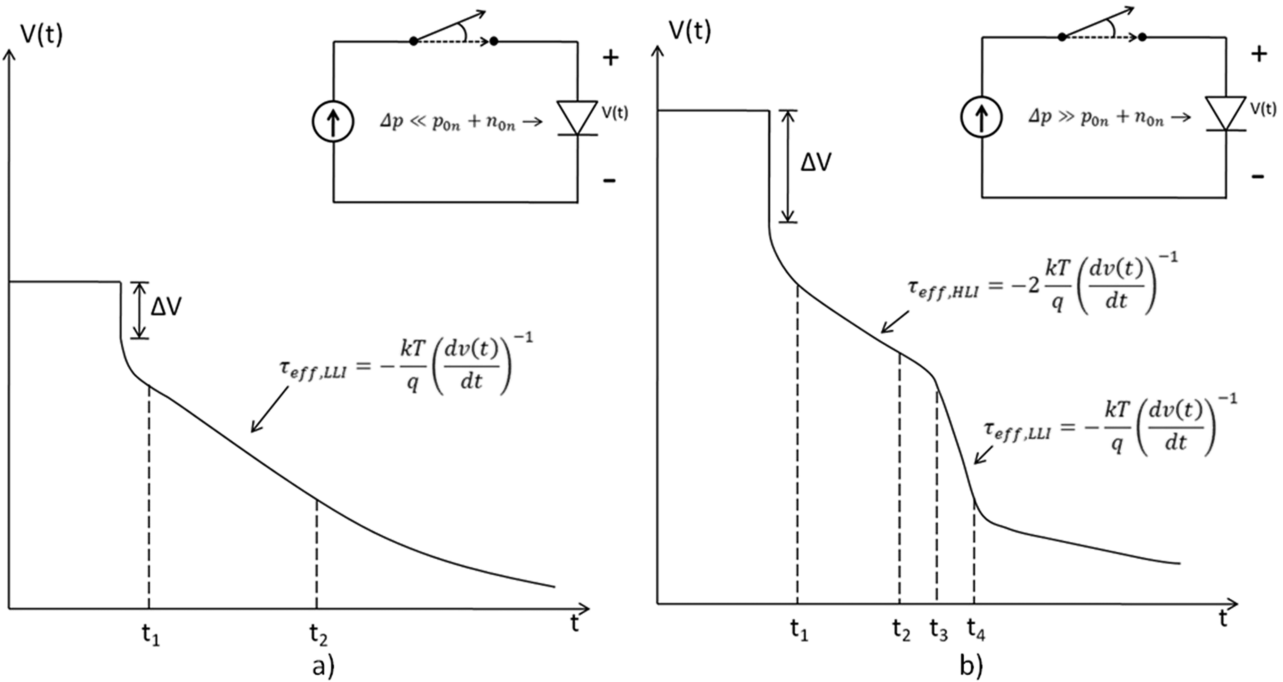


FIG. 2. Ideal OCVD waveforms. (a) Ideal LLI decay waveform and circuit. (b) Ideal HLI decay waveform and circuit.

This factor ranges in value from 1 at low injection [$\Delta p \ll (n_0 + p_0)$] to 2 under high injection levels [$\Delta p \gg (n_0 + p_0)$]. Figure 2(a) displays an ideal Low Level Injection (LLI) circuit and decay waveform, and Fig. 2(b) displays the High Level Injection (HLI) condition and waveform, along with the relevant portions of the decay waveform^{13–15} where Eq. (9) is applicable for extracting the effective lifetime.

As can be seen from Fig. 2(b), under high level injection, the decay waveform exhibits two distinct linear segments [portions where $F(t)$ is constant], from which both the LLI and HLI lifetimes can be extracted.

III. WIDE INJECTION RANGE OPEN CIRCUIT VOLTAGE DECAY SYSTEM

The system described in this work was designed specifically to perform the OCVD technique over a range of current from 1 mA up to 200 A. This range of over six orders of magnitude of current, and hence carrier injection, was implemented to allow the system to acquire IDLS curves over a wide range instead of arbitrarily chosen LLI and HLI levels. This wide span of current also allows a range of devices from small-signal to power devices to be evaluated with a single piece of equipment. Being able to acquire an entire IDLS curve allows a researcher to see potential errors in correlating a τ_{eff} measurement with the actual SRH lifetime due to any recombination event external to the most dominant center, e.g., the onset of Auger recombination or the effect of a second recombination center that becomes more efficient at elevated injection levels. Factors such as these would invalidate the use of LS methods as they are based on the SRH formalism being applied to a single dominant defect.

A. OCVD system hardware

In order to perform the OCVD technique as accurately as possible over a very wide injection range without large parasitic elements affecting the measurement and without causing joule heating of the junction in the higher injection regimes, a custom unit was designed and built for the work performed herein. The parameters for the system are summarized as follows.

- A high current, controllable source for current injection that can operate in a pulsed manner to avoid joule heating which would alter the measurement.
- An electronically controlled, fast, nearly ideal switch to disconnect the device under test (DUT).
- A voltage measurement system with widely variable sampling rates.
- A current measurement system capable of monitoring ~ 1 mA – 200 A.
- Software that circumvents the inherent abstraction of the lifetime caused by heavy filtering and differentiating of the OCVD waveform(s).
- A controllable parallel resistance to compensate for parallel capacitance if needed.

All of these requirements are incorporated into the unit designed, a block diagram of which is shown in Fig. 3.

The system applies a controlled voltage pulse through a high-power (2 kW) linear amplifier fed by low ESR capacitors that are charged from a low power voltage source of 12 V. Three Insulated-Gate Bipolar Transistors (IGBTs) in parallel are used to form a high current series pass element that is controlled by a high gain feedback amplifier. This amplifier is in turn fed by a 10-bit Digital to Analog Converter (DAC) that receives data from the system's microcontroller,

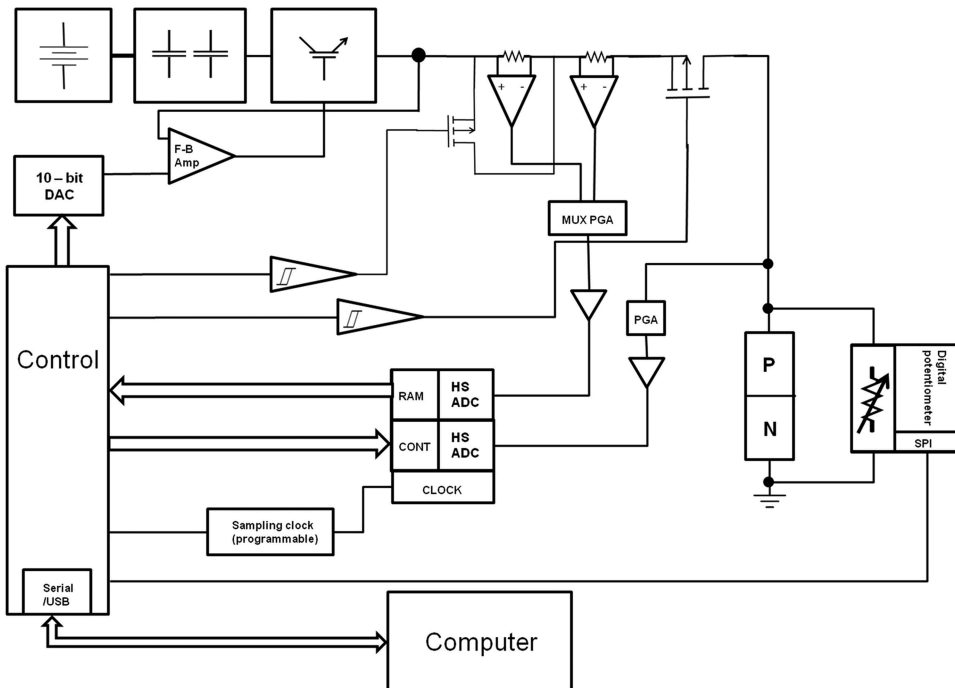


FIG. 3. OCVD system block diagram.

a Microchip PIC 18F6585 via an SPI protocol. The voltage waveform at the output terminals (the pn junction voltage) is acquired through a differential amplifier, a Programmable Gain Amplifier (PGA), and then fed into a high speed Analog to Digital Converter (ADC) with built-in RAM memory. The voltage read-in ADC has a separate, programmable clock that is controlled by the Micro Controller Unit (MCU) and can range from ~ 1 MHz to 200 MHz. In series with the pn junction is a low Resistance Drain to Source (RDS)-on MOSFET that is used to disconnect the pn junction quickly from the driving source and two precision shunt resistors that acquire the current waveform. One of the shunt resistors is paralleled with another low RDS-on MOSFET to read relatively low current levels and give the system a wide range of measurable injected current with relatively good resolution. These current shunts are attached to two differential amplifiers that are fed through a multiplexer into another PGA and high speed ADC/RAM unit. The addition of a relatively high-voltage analog multiplexer on the output terminals gives the user the ability to add programmable parallel resistance to the pn junction being evaluated in order to compensate for the device system or cabling capacitances. Figure 4 shows the physical OCVD unit.

B. OCVD system software

A Graphical User Interface (GUI), written in Visual Basic, was implemented to send commands to the OCVD system and collect data and waveforms for display and manipulation. A user can initiate a single set voltage pulse, acquire the resultant voltage and current waveforms, set limits (compliance) for voltage and current, and then perform an IV sweep with a current range from millamps to 200 A and to 10 V. Alternatively, the user can specify a current injection level and the system will pulse this current for approximately 100 μ s, followed by

initiation of a voltage read and subsequent disconnection of the attached pn junction. The voltage waveform thus obtained is displayed on the screen along with the actual current injection level read by the unit. For any of these functions, data can be saved as both a Comma Separated Value (CSV) and an image file.

As stated in Sec. II, to calculate the effective carrier lifetime from the OCVD waveform, the slope of the voltage decay during a representative linear segment must be extracted. The most common method used to extract this slope is to filter the raw data and then perform numerical differentiation on the extracted data.¹⁶ While this method is theoretically viable for OCVD lifetime extraction, actual implementation across a broad signal spectrum is difficult to obtain; real life data are inherently noisy, and the act of differentiation increases the level of noise in the data (hence the pre-filtering method). Filtering, however, further abstracts the actual data from the original signal. In addition, the level of the initial voltage drop due to series resistance of a pn junction can be significant



FIG. 4. Wide injection range OCVD system.

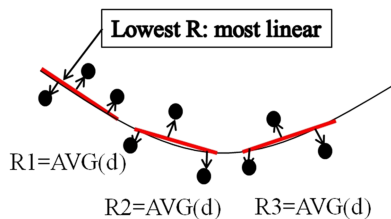


FIG. 5. Most-linear segment algorithm applied to an example curve.

in high-voltage PIN devices; if this drop is several volts in magnitude, and the sought-after signal slope changes by a few millivolts, the derivative can be hard to obtain by numerical differentiation.

To circumvent these issues associated with the extraction of the decay waveform's slope, a unique algorithm was designed that works directly with the empirical data set(s) acquired. The algorithm is based on a line segment of chosen length (number of data points) that "slides" along the data set within an arbitrarily chosen interval. The line segment is calculated via the linear least-squares method at each point along its path on the interval. At each position, the average distance from the line to each data point also in the interval is calculated and used as a figure of merit for the linearity of that particular segment. In this way, the actual slope is calculated instead of a number that is removed from the slope by the filtering and differentiating processes. The unique algorithm presented here is effectively a precise automated variation of the very first hand-applied technique used by Lederhandler and Giacoletto. Figure 5 shows the basic method of the algorithm acting on a curve.

Once the algorithm finds the most linear segment, the slope is recorded. This is the dv/dt required for the lifetime calculation. The software (currently a separate program from the OCVD GUI) calculates the effective lifetime from this slope, the temperature (entered as degrees Kelvin), and whether the decay is from low level or high level injection.

C. OCVD system verification and calibration

The prototype OCVD system has undergone basic functionality testing including IV curve tracing from very low mA ranges to 200 A with good results. Initial OCVD waveforms were taken with various small signal Si pn junction diodes in order to compare the results with theoretical decay waveforms (Fig. 2). Figure 6(a) shows the graph taken from the prototype system with a small signal diode with a current injection of approximately 80 mA, while (b) is the data taken from another diode under HLI conditions. This graph displays the distinct dual linear segments representing HLI and LLI. These two graphs come from a series of injection levels that only require a user to enter a desired current level. This allows the evolution of the decay waveform to be viewed over several orders of magnitude, which helps in revealing when HLI is reached and when Auger recombination might become a factor and also helps reveal any potential secondary center effects. All data sets are saved as both image files and CSV files.

IV. APPLICATION OF LS TECHNIQUES TO A COMMERCIAL HV PIN DIODE

The wide injection range OCVD system described in Sec. III has been used to perform simple high/low τ_{eff} studies and single IDLS sweeps and, in conjunction with a commercial temperature chamber, to perform the advanced T-IDLS techniques outlined in Sec. II on a commercial 1N4007 1 kV PIN diode. The results of this work are described in Secs. IV A–IV C.

A. LLI and HLI studies

The OCVD system was used with the 1N4007 PIN diode to initially measure the effective lifetime under both LLI and HLI conditions. The LLI level was measured with an injected current of ~ 100 mA, and the HLI range was extracted with an injected current of ~ 5 A, both of these injection levels

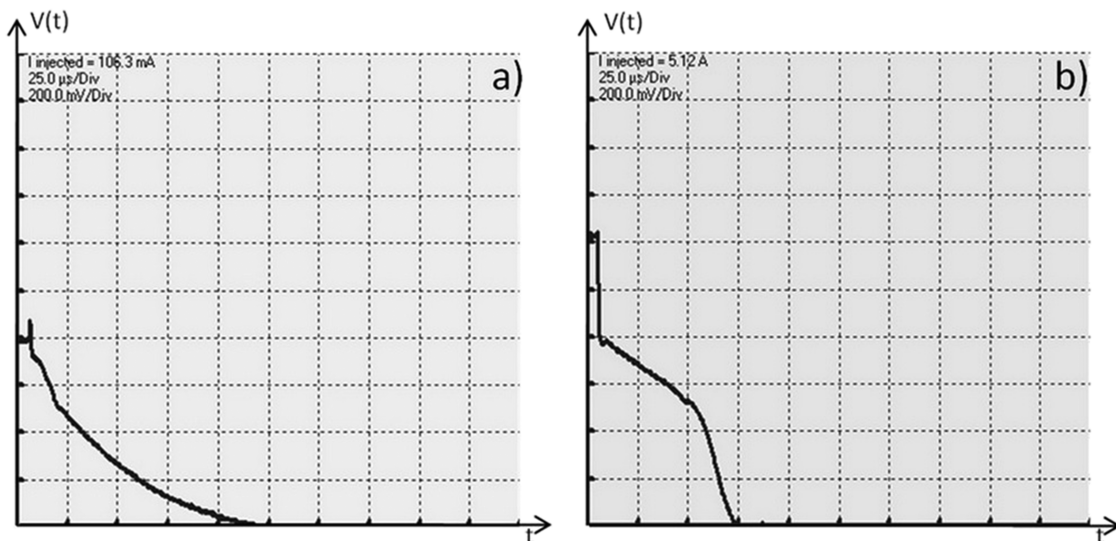


FIG. 6. Empirical LLI (a) and (b) HLI decay waveforms.

were chosen from stable portions of an IDLS curve with injection ranging over 4 orders of magnitude. The actual effective lifetime was acquired with the extraction software detailed in Sec. III. For the particular device used in the T-IDLS work that follows, the LLI lifetime was measured as $3.2 \mu\text{s}$ and the HLI lifetime as $7.6 \mu\text{s}$ at 300 K. Several 1N4007 diodes displayed LLI and HLI lifetimes ranging from 3.0 to $3.5 \mu\text{s}$ and 7.4 to $8.5 \mu\text{s}$, respectively.

One single work in the literature was found that also performed simple LLI/HLI lifetime studies using the same model diode.¹⁷ The results for LLI ranged from $3.4 \mu\text{s}$ to $4.0 \mu\text{s}$, while the HLI lifetime ranged from $8.3 \mu\text{s}$ to $10.0 \mu\text{s}$. Considering the possible variations in the diodes used due to manufacturers and differences in the physical setup of the experiment and the lifetime extraction methods between this work and that cited, the agreement in measurements is relatively good.

B. IDLS studies

The work that follows, to the authors' knowledge, are the first studies performed on a commercial packaged device using the advanced IDLS and T-IDLS techniques. A 1N4007 HV PIN diode was subjected to a series of increasing current injection levels to obtain data for a single IDLS sweep. For these measurements, the temperature was 300 K (approximately room temperature). The currents injected into the device were 0.01, 0.05, 0.1, 0.5, 1.0, and 5 A. To calculate the injection ratio (η), the simple relation in Eq. (11) was used,¹⁸

$$\Delta n_p = \frac{n_i^2}{N_A} \left(e^{\frac{qV_A}{kT}} - 1 \right). \quad (11)$$

This is viable only under LLI conditions and as such was used at the low injection levels by measuring the applied voltage. Once this baseline for LLI injected carriers was found using Eq. (9), the injection ratio could be found for each current step as it scales approximately in proportion with the current.

One additional piece of information is required to graph an IDLS sweep: the doping concentration must be known. As these data were not available for the diode used, a maximum value was calculated based on the device's breakdown voltage using the following equation:¹⁹

$$N_A = \left(\frac{B_V}{5.34 \times 10^{13}} \right)^{\frac{3}{4}}. \quad (12)$$

From this, a value of $2 \times 10^{14} \text{ 1/cm}^3$ was extracted. While a lower doping is possible for a breakdown of 1 kV, it would increase the "on" resistance of the device, a practice that is avoided whenever possible.

The data are then plotted in Fig. 7 as a single IDLS sweep. From the graph, the IDLS curve is increasing with injection, which seems to be indicative of a deeper or at least not a shallow level defect.

C. Advanced T-IDLS DPSS studies

The advanced T-IDLS techniques were applied next in an attempt to obtain discrete solutions for the material parameters associated with the dominant recombination center.

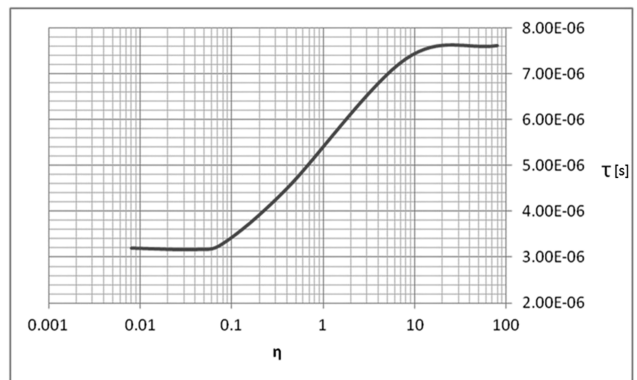


FIG. 7. IDLS curve from extracted data.

The objective of sweeping the temperature through a given range in T-IDLS is to vary the SRH densities, n_1 or p_1 , enough to alter the shape of one or more of the IDLS curves, which can then theoretically give discrete intersection points (E_t) on an overlay of the DPSS- k graphs generated at each temperature. In order to change the SRH densities enough to alter the shape of such a curve without the sample device suffering from either freeze-out or the onset of too many intrinsic carriers at the low and high temperature extremes respectively, the carrier concentration was calculated using the doping concentration of $2 \times 10^{14} \text{ 1/cm}^3$ and is normalized and graphed in Fig. 8.

From this, a range of 250 K–400 K was chosen as minimum and maximum temperatures. An MPI ThermalAir unit was used to achieve the desired temperature sweeps, with a temperature probe directly connected to the 1N4007 diode to provide feedback to the unit.

The temperature applied to the 1N4007 diode was increased from the low range of 250 K in steps of 50 K increments; Table I lists the results from the lifetime extraction over the injection range at each temperature step.

With the four sets of data acquired from the temperature sweeps performed, the DPSS- k and DPSS- τ_{n0} graphs were constructed for each temperature value, and all of these curves were overlaid into a single graph of each DPSS quantity. As the symmetry factor is theoretically constant over temperature due to the thermal velocity and capture coefficients

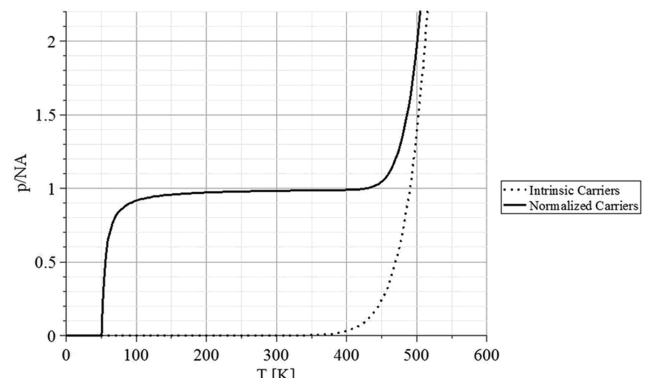


FIG. 8. Normalized carrier concentration vs. temperature.

TABLE I. Results of temperature sweeps.

| 250 K | | | 300 K | | | 350 K | | | 400 K | | |
|---------|--------|-----------------------|---------|--------|-----------------------|---------|--------|-----------------------|---------|--------|-----------------------|
| current | η | τ |
| 0.0112 | 0.008 | 2.42×10^{-6} | 0.01063 | 0.008 | 3.20×10^{-6} | 0.01142 | 0.008 | 4.22×10^{-6} | 0.01142 | 0.008 | 6.20×10^{-6} |
| 0.0559 | 0.04 | 2.48×10^{-6} | 0.05197 | 0.04 | 3.17×10^{-6} | 0.05315 | 0.04 | 4.50×10^{-6} | 0.05315 | 0.04 | 6.20×10^{-6} |
| 0.101 | 0.08 | 2.79×10^{-6} | 0.1004 | 0.08 | 3.30×10^{-6} | 0.101 | 0.08 | 4.75×10^{-6} | 0.101 | 0.08 | 6.35×10^{-6} |
| 0.532 | 0.4 | 3.55×10^{-6} | 0.504 | 0.4 | 4.50×10^{-6} | 0.504 | 0.4 | 5.40×10^{-6} | 0.504 | 0.4 | 8.00×10^{-6} |
| 1.01 | 8 | 5.25×10^{-6} | 1 | 8 | 7.33×10^{-6} | 1 | 8 | 9.00×10^{-6} | 1 | 8 | 1.16×10^{-5} |
| 5.12 | 80 | 5.85×10^{-6} | 4.88 | 80 | 7.62×10^{-6} | 5.12 | 80 | 1.00×10^{-5} | 5.12 | 80 | 1.20×10^{-5} |

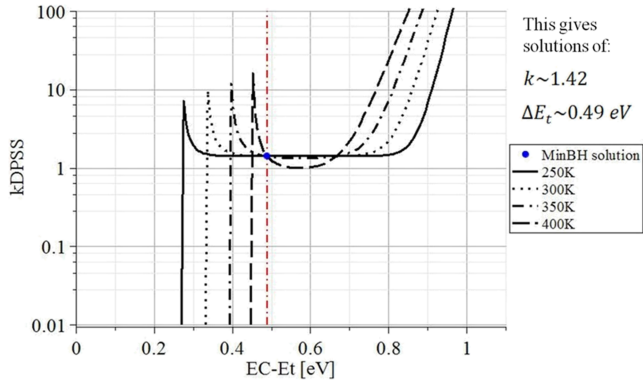


FIG. 9. MinBH solution of the T-IDLS DPSS-k graph.

changing in the same manner for either minority or majority capture, this graph was used to find the absolute energy depth of the dominant recombination center |Et|. This numerical solution for the DPSS-k curves is shown in Fig. 9, with the value being equal to approximately 0.49 eV below the conduction band and above the valence band. This solution then gives a symmetry factor of ~ 1.42 .

The next step in identifying the parameters of the defect is to use the numerical value for Et obtained from the DPSS- τ_{n0} graphs to extract values of the minority carrier lifetime at each discrete temperature step. These minority lifetime values should vary with a square law as given in Sec. II, Eq. (8). This is performed in Fig. 10 for the extracted Minority Band Half (MinBH) solution of 0.49 eV.

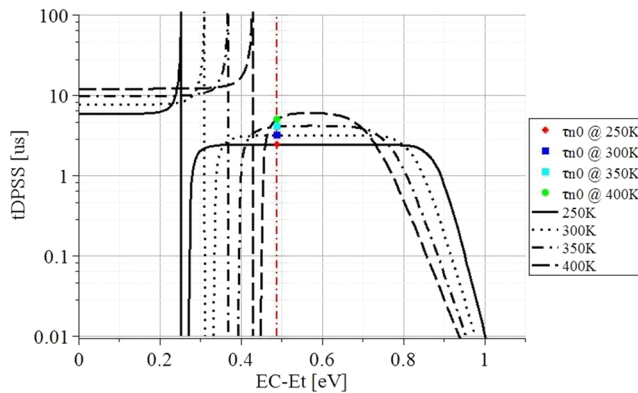
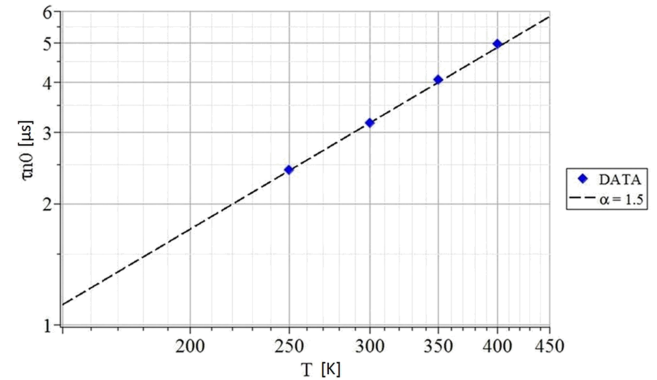
FIG. 10. Discrete values for τ_{n0} at $Et = 0.49 \text{ eV}$.

FIG. 11. Empirical data and Eq. (12).

With these empirically extracted minority carrier lifetime values, it is a simple matter to use Eq. (8) to solve for the exponent, which gives the minority carrier lifetime, τ_{n0} , as a function of temperature,

$$\tau_{n0}(T) = 3.17 \times 10^{-6} \left(\frac{T}{300} \right)^{1.5}. \quad (13)$$

To verify this relationship, Fig. 11 displays the extracted τ_{n0} values in a logarithmic graph with Eq. (13) overlaid. The alignment of the data with this function shows a very good correlation.

At this point, every parameter of the defect that directly relates to its recombination activity has been extracted. To check these results, the extracted values are placed in the full SRH equation and the equation is then graphed over a viable injection range for each temperature at which data were

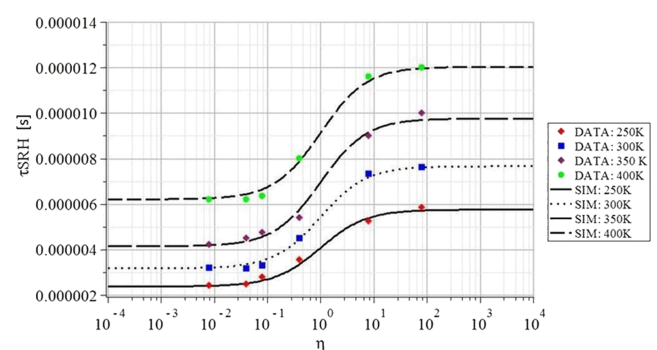


FIG. 12. Simulated IDLS curves and empirical data.

acquired and the data itself are then overlaid on the same graph. This is performed in Fig. 12. It can be seen from the graphs that the simulation and the empirical data are in good agreement with each other.

Finally, the results can be viewed in terms of known defects to help evaluate the plausibility of the parameters extracted from the experiment. Referencing a table or graph of the known energy levels introduced by various elements in Si (e.g., Ref. 18), one finds that there are three elements that lie at an absolute energy depth of 0.49 eV. Of these three elements, vanadium is known in the semiconductor industry as one of three major contaminants plaguing modern Si devices and also as one of the most active recombination centers in Si.²⁰

V. CONCLUSION

A wide current injection range OCVD system was designed with built-in data capture. This complete, stand-alone unit is not plagued by noise introduced from the excessive resistance and inductance found in OCVD systems made from disparate pieces of equipment. A range of over six orders of magnitude of carrier injection is available, with the chosen current level simply being entered into a GUI. Unique algorithms have been written to extract the effective carrier lifetime directly from the empirical data acquired. The very first IDLS and T-IDLS studies (to the authors' knowledge) were performed on a packaged commercial 1N4007 PIN HV diode. The T-IDLS methods were able to extract reasonable values for the minority carrier lifetime as a function of temperature, the symmetry factor, and the absolute energy depth of the dominant defect. The results were simulated using the full SRH equation at the relevant temperatures and found to correlate with the data with a high degree of accuracy. The energy depth extracted was compared to the known contaminants in Si and seemed to line up with a common element known for its high recombination activity and for plaguing modern devices.

ACKNOWLEDGMENTS

We would like to thank the Army Research Laboratory (Contract No. W911NF-14-2-0069) for supporting this work and for lending their technical expertise.

- ¹A. Salemi *et al.*, "Conductivity modulated on-axis 4H-SiC 10+ kV PiN diodes," in *2015 IEEE 27th International Symposium on Power Semiconductor Devices & IC's (ISPSD)* (IEEE, Hong Kong, 2015), pp. 269–272.
- ²A. A. Ogunniyi *et al.*, "Analysis of carrier lifetime effects on HV SiC PiN diodes at elevated pulsed switching conditions," in *2015 IEEE Pulsed Power Conference (PPC)* (IEEE, Austin, TX, 2015), pp. 1–6.
- ³M. E. Levenshtein *et al.*, "'Paradoxes' of carrier lifetime measurements in high-voltage SiC diodes," *IEEE Trans. Electron Devices* **48**(8), 1703–1710 (2001).
- ⁴D. V. Lang, "Deep-level transient spectroscopy: A new method to characterize traps in semiconductors," *J. Appl. Phys.* **45**(7), 3023–3032 (1974).
- ⁵S. W. Glunz *et al.*, "Minority carrier lifetime degradation in boron-doped Czochralski silicon," *J. Appl. Phys.* **90**(5), 2397–2404 (2001).
- ⁶S. Rein, *Lifetime Spectroscopy: A Method of Defect Characterization in Silicon for Photovoltaic Applications* (Springer, 2005).
- ⁷S. Bellone, G. D. Licciardo, G. Guerriero, and A. Rubino, "An analytical model of an OCVD-based measurement technique of the local carrier lifetime," *IEEE Trans. Electron Devices* **54**(11), 2998–3006 (2007).
- ⁸M. E. Levenshtein, T. T. Mnatsakanov, P. A. Ivanov, R. Singh, K. G. Irvine, and J. W. Palmour, "Carrier lifetime measurements in 10kV 4H-SiC diodes," *Electron. Lett.* **39**(8), 689–691 (2003).
- ⁹M. Derdouri, P. Leturcq, and A. Munoz-Yague, "A comparative study of methods of measuring carrier lifetime in p-i-n devices," *IEEE Trans. Electron Devices* **27**(11), 2097–2101 (1980).
- ¹⁰E. Van Brunt, A. Agarwal, A. Burk *et al.*, "A comparison of the microwave photoconductivity decay and open-circuit voltage decay lifetime measurement techniques for lifetime-enhanced 4H-SiC epilayers," *J. Electron. Mater.* **43**, 809 (2014).
- ¹¹S. Bellone and G. D. Licciardo, "An analog circuit for accurate OCVD measurements," *IEEE Trans. Instrum. Meas.* **57**(6), 1112 (2008).
- ¹²S. Lederhandler and L. Giacoletto, "Measurement of minority carrier lifetime and surface effects in junction devices," *Proc. IRE* **43**(4), 477–483 (1955).
- ¹³H. Schlangenotto and W. Gerlach, "On the post-injection voltage decay of P-S-N rectifiers at high injection levels," *Solid-State Electron.* **15**(4), 393–402 (1972).
- ¹⁴R. Gopal, R. Dwivedi, and S. K. Srivastava, "Open-circuit voltage-decay behavior in P-N junction diode at high injection," *J. Appl. Phys.* **58**(9), 3476–3480 (1985).
- ¹⁵M. Tapajna, J. Pjencak, A. Vrbicky, P. Kudela, and L. Harmatha, "Application of open circuit voltage decay to the characterization of p/n+ and n/p+ epitaxial layer," *Adv. Electr. Electron. Eng.* **3**(2), 265–268 (2011).
- ¹⁶D. K. Schroder, *Semiconductor Material and Device Characterization* (John Wiley & Sons, New York, 2006).
- ¹⁷S. Montero, A. P. Cedola, M. A. Cappelletti, and E. L. P. y Blanca, *A Computerized Method for Carrier Lifetime Measurement in PN Junctions at High and Low-Level Injection* (Argentine School of Micro-Nanoelectronics Technology and Applications (EAMTA), Montevideo, 2010), pp. 87–93.
- ¹⁸R. F. Pierret, *Advanced Semiconductor Fundamentals* (Addison-Wesley Publishing Company, Reading, Massachusetts, 1987).
- ¹⁹B. Jayant Baliga, *Fundamentals of Power Semiconductor Devices* (Springer, New York, 2008).
- ²⁰V. A. Perevostchikov and V. D. Skupov, *gettering Defects in Semiconductors* (Springer, Berlin, 2005).